Dynamics of *bicoid* mRNA localisation and translation dictate morphogen gradient formation

T. Athilingam[1,+], E.L. Wilby[2,+], P. Bensidoun[3], A. Trullo[3], M. Verbrugghe[3], X. Shi[2], M. Lagha[3], T.E. Saunders[1,*], T.T. Weil[2,*]

[1] Warwick Medical School, University of Warwick, Coventry, CV4 7AL, United Kingdom
[2] Department of Zoology, University of Cambridge, Cambridge, CB2 3EJ, United Kingdom
[3] Institut de Génétique Moléculaire de Montpellier, Univ Montpellier, CNRS, Montpellier, France.

[+] Equal contribution, listed alphabetically
[*] For correspondence: timothy.saunders@warwick.ac.uk, tw419@cam.ac.uk

Abstract

The transcription factor Bicoid (Bcd) protein guides early *Drosophila* patterning and is the best-characterised morphogen. The source of the morphogen, *bcd* mRNA, is maternally deposited during oogenesis and localised to the anterior pole of the mature oocyte. While the spatiotemporal interpretation of the Bcd morphogen gradient has been intensely studied, when and where Bcd protein is produced and how this protein gradient is dynamically shaped remains contentious. Here, we use the SunTag reporter system to quantitatively examine the spatiotemporal profile of *bcd* mRNA translation *in vivo*. We show that association with Processing bodies (P bodies) in mature oocytes prevent premature *bcd* mRNA translation. Following egg activation, *bcd* mRNA dissociates from P bodies and translation is observed at the anterior pole. Translation remains restricted to the anterior domain throughout early development, even after nuclear migration in the syncytial blastoderm. At cellularisation, translation ceases and the remaining *bcd* mRNA associates with reformed P bodies, which appear to block any further translation. We use these observations to create a new modified source-diffusion-degradation model of Bcd gradient formation that has spatiotemporally varying production. Overall, our study reveals that *bcd* mRNA translation is tightly controlled in space and time during oogenesis and early embryogenesis.

Key words

Morphogen, mRNA regulation, body-axis patterning, P bodies, translation

Introduction

The concept of signalling molecules, coined morphogens, was proposed by Turing (1). These molecules help guide spatial patterning by varying in concentration across developing systems. Downstream target genes respond in a concentration-dependent manner to the morphogen gradient (2). Bicoid (Bcd) protein is a transcription factor found in the early *Drosophila* blastocyst and was the first morphogen gradient identified (3). A concentration gradient of Bcd extends along the anterior-posterior (AP) axis from highest at the anterior pole of the embryo and reaches around 70% of the embryo's length. The expression of target genes, like *hunchback,* depends on the local Bcd concentration (4-6).

Shortly after its discovery, the Synthesis, Diffusion, Degradation (SDD) model was introduced to explain how the Bcd gradient forms (3, 7). This model assumed that Bcd is produced at the anterior pole, then diffuses through the embryo and is subsequently degraded. The model predicted a concentration profile that decreased exponentially in steady state, consistent with *in vivo* observations (7-9). There are several mechanisms that can create morphogen profiles that decay exponentially (10, 11). Alternatives to the SDD model include: (i) local production of Bcd protein by *bcd* mRNA spatially distributed along the embryo (12); (ii) early translation of *bcd* in the oocyte which would allow the Bcd morphogen to spread quickly before patterning happens in later nuclear cycles (13); and (iii) nuclear dilution, which does not require protein degradation (14). These models predict different times and places for *bcd* mRNA translation. Still, they can all create exponential-like concentration gradients under the right conditions and time scales for patterning (15-17).

Localised *bcd* mRNA first appears at the anterior region in mid-stage oocytes (18-20). As oogenesis progresses, *bcd* transitions from a continual active transport to stable anchoring at the anterior cortex (20, 21). By the end of oogenesis, the mature oocyte (stage 14) is endowed with all the *bcd* needed for anterior patterning in the embryo (18-21). There is no biochemical evidence that *bcd* translation happens before egg activation (22-24), a conserved process that triggers several major changes in the egg (25-28). These changes include restarting meiosis, altering the translational landscape, and reconfiguring the cytoskeleton. These events occur as the mature egg moves into the oviduct before fertilisation in the uterus (29). Translational repression of *bcd* in the oocyte is proposed to occur through its association in a ribonuclear protein (RNP) granule, a class of biomolecular condensates (30, 31).

Most research on biomolecular condensate composition, physical properties, and function has focused on single cell models and *in vitro* systems (32-36). This provides an excellent basis

for studying ribonucleoprotein (RNP) granule physiology and translational regulation in multicellular organisms. Genetic and physical manipulation in *Drosophila* have recently helped us understand the biological relevance of RNP granules in a developmental context (37-41). For example, visualising *nanos* mRNA translation shows that germ granules can either be sites of translation or repression depending on the location of the mRNA (40, 41). Also, the germ-line determinant *oskar* (*osk*) mRNA associates with “solid-like” condensates where its unique secondary structure is required to maintain *osk* mRNA inside the condensates, where it is translationally repressed (37).

A similar model of mRNA regulation via association with an RNP granule had previously been proposed for *bcd* mRNA (30, 31). Once localised to the anterior, *bcd* is sequestered in the core of Processing bodies (P bodies) away from ribosomes (30). P bodies are an evolutionarily cytoplasmic RNP granule. Depending on the cellular context, they are implicated in storing and degrading mRNA (32, 42). A variety of proteins that help regulate mRNA are enriched in P bodies including the DEAD-box family RNA helicase, Maternal Effect at 31B (Me31B). It has homologies with proteins in other species: DDX6 in humans, Dhh1 in *S.cerevisiae*, Xp54 in *Xenopus*, and Cgh-1 in *C.elegans* (30, 43). Previous work has shown that Me31B functions both in repression and clearance of maternal transcripts in early *Drosophila* embryogenesis (44).

Previous studies on the Bcd morphogen gradient have mainly looked at two areas. One focuses on the regulation of *bcd* mRNA during oogenesis (30, 45-47). The other examines Bcd protein dynamics after translation (7, 10, 17, 48, 49). To fully understand how the Bcd gradient forms, we need to integrate these two approaches. Here, we used the SunTag/scFv imaging-based reporter system (50-57) to quantitatively assay *bcd* translation in *Drosophila* oocytes and embryos. We show that *bcd* mRNA is not translated when it is in P bodies at the end of oogenesis. Following egg activation, or experimentally driven disassociation, *bcd* is no longer in P bodies and is translated. We observed *bcd* translation starts quickly after release from P-bodies, but it happens only at the anterior pole of the embryo. After nuclear migration, *bcd* localisation appears dispersed though the location of translation remains unchanged. We saw a decrease in *bcd* translation in nuclear cycle (n.c.) 11 onwards, consistent with observations from assaying the protein levels (58). Motivated by our experimental observations, we demonstrate that a modified SDD model, with spatially and temporally varying Bcd production, is consistent with our results.

Results

bcd translation begins after egg activation

To test when and where *bcd* mRNA is translated, we generated a *SunTag-bcd* transgene, containing an array of 32 SunTag GCN4 repeats (*bcdSun32*) (Figure 1A, Methods). We first validated our reporter in early embryos, where Bcd protein is known to be present (59). We performed fluorescence single molecule *in situ* hybridisation (smFISH) to label *bcdSun32* and antibody labelling to visualise the SunTag nascent peptide (Figure 1B). We verified the *bcdSun32* reporter by showing two populations of *bcdSun32* particles: *bcdSun32* mRNA particles co-localizing with the GCN4 antibody signal, (implying polysome and mRNA engaged in translation); and *bcdSun32* mRNA molecules that do not overlap with anti-GCN4 (not in translation) (Figure 1B). We also performed this validation using the fluorescent detector, the single-chain antibody scFV, which is genetically encoded and maternally provided (*nos-scFv-MSGFP2*) (60). To further test the reporter, we expressed *bcdSun32* in oocytes. We observed no translation in oocytes (Figure 1C-D) which matches what we predicted from earlier findings of *bcd* mRNA translational regulation (61, 62).

Previous work on P bodies has shown they do not contain ribosomes and can act as sites of mRNA storage (63-65). To test if *bcd* mRNA is translationally repressed when in P bodies, we calculated the amount of *bcd* mRNA co-localisation to P bodies. We focused on the developmental transition from the mature egg to the early embryo. Our previous qualitative data postulated that location in P bodies is key for controlling *bcd* translation (31). Using single molecule fluorescence *in situ* hybridisation (smFISH) and the standard P body marker Me31B, we confirmed that *bcd* is in P bodies before egg activation (Figure 1E-F). Then, during the transition from a mature oocyte to activated egg, P bodies disassembled and *bcd* was no longer co-localised with P bodies (Figure 1E-F) (30, 31). We also confirmed that *bcd* becomes dispersed, losing its tight association with the anterior cortex (Figure 1E) (31). In the early embryo, the distribution of *bcd* stayed the same while ‘embryonic' P bodies formed (Figure 1E). There was no co-localisation detected between *bcd* and P bodies at this stage, consistent with past work showing that the re-formed P bodies have different traits compared to those in the oocyte (Figure 1F) (31).

We next show that disrupting the calcium wave in the activated egg caused a failure to disperse P bodies during *ex vivo* egg activation (Figure 1E). In these activated eggs, *bcd* mRNA remains co-localised with the retained P bodies (Figure 1F). While addition of the chemical NS8593 disrupts the calcium wave, other phenotypic markers of egg activation are still observed (58). Based on these results and previous observations (31, 66), we

140 hypothesised that the loss of co-localisation between *bcd* and P bodies correlates with *bcd*
141 translation.
142
143 To test this model, we used the *bcdSun32* to observe translation during this transition. Before
144 egg activation, Bcd protein was not detected (Figure 1G-H). However, after egg activation,
145 *bcd* mRNA translation occurred rapidly and continued after egg laying (25, 67) (Figure 1G-H).
146 Consistent with previous findings, we only observed *bcd* translation at the anterior of the
147 activated egg and early embryo (Figure 1G-H) (3, 68). Furthermore, we did not see *bcd*
148 translation in NS8593 treated activated mature eggs (Figure 1G-H). This means that the P
149 bodies likely serve as a barrier, keeping *bcd* transcripts within a translation-free environment
150 in the oocyte.
151
152 **Premature release of *bcd* mRNA results in ectopic translation**
153 Altering the physical state of an RNP granule can impact its ability to store mRNA (31, 37, 69).
154 To further test if *bcd* storage in P bodies is required for translational repression, we monitored
155 mRNA association with P bodies after chemical treatment known to disrupt P body integrity
156 (31, 70-72). After treating mature oocytes with these solutions, we observed BcdSun32 protein
157 in the oocyte anterior (Figure 2A-B). We checked the treated mature eggs for egg activation
158 markers to ensure that the chemical treatment did not trigger activation, which could cause
159 translation (73). Chemically treated eggs failed the activation test of bleaching for two minutes
160 (74). This confirms that the storage in P bodies is crucial to maintain *bcd* translational
161 repression (31).
162
163 To further test this model, we used mutations in *Drosophila* Endosulfine (Endos), which is part
164 of the conserved phosphoprotein α-endosulfine (ENSA) family (75). This caused a change in
165 RNP granule phenotype after oocyte maturation, similar to that observed with chemical
166 treatment (Figure 2C) (31). This temporal effect matched the known roles of Endos as the
167 master regulator of oocyte maturation (75, 76). *endos* mutant oocytes lost the co-localisation
168 of *bcd* and P bodies, concurrent with P bodies becoming less viscous during oocyte maturation
169 (Figure 2D, Figure S1). Particle size and position analysis showed that *bcd* mRNA prematurely
170 exhibits an embryo distribution in these mutants (Figure 2E). Due to genetic and antibody
171 constraints, we are unable to test for translation of *bcd* in the *endos* mutant. However, it follows
172 that *bcd* observed in this diffuse distribution outside of P bodies would be translationally active
173 (Figure 2E-F).
174

175 ***bcd* mRNA translation is spatially restricted during early *Drosophila* embryogenesis**
176 We next addressed when and where the embryo translates *bcd* mRNA, if *bcd* translation is
177 limited to the anterior pole, and when does the maximum translation occur. We considered
178 that the size of *bcdSun*32 may impede mRNA biogenesis and the function of the protein as a
179 transcription factor. Therefore, we generated a second transgene with ten GCN4 repeats
180 (*bcdSun10*) (Figure S2). Importantly, *bcdSun10* rescued the bcd^{E1} null mutant suggesting that
181 the tag does not greatly affect function (Figure S2). Immuno-smFISH for GCN4 and *bcd*
182 revealed translating and non-translating *bcd* particles in the anterior pole of the embryo (Figure
183 3). Individual *bcd* particles (inferred from diffraction limited spots) colocalised with varying
184 intensities of translating bcd-SunTag nascent proteins (Figure S3). At n.c.4, we saw a strong
185 link between *bcd* mRNA and translation sites in the anterior, with most translation events
186 happening within 100 μm of the anterior pole on the dorsal surface, and no translation
187 observed more than 100 μm from the anterior pole (Figure 3B-C). The Bcd protein gradient is
188 known to have small but reproducible differences between dorsal and ventral surfaces (4).
189 Consistent with this, the translation profile differed between the dorsal to ventral sides, likely
190 due to the asymmetric *bcd* spread on the DV-axis and on their surfaces (Figure 3A-A'' lower
191 panels, Figure S4).
192
193 We next quantified the number of translation events in different regions of n.c. 4 embryos
194 (Methods, Figure S3). In the anterior region of the dorsal surface, less than 50 μm from the
195 pole, above 90% of *bcd* particles are engaged in translation (Figure 3C-C'). Over 98% of all
196 observed translation events occurred within 75 μm of the anterior pole on the dorsal side, with
197 almost none seen beyond 100 μm as the *bcd* numbers are negligible. Overall, we see
198 consistent translation efficacy irrespective of spatial differences. We conclude that during early
199 embryogenesis, before nuclear migration to the cortex, *bcd* translation only occurs in the
200 anterior region and mirrors the anterior-localised *bcd* distribution.
201
202 **Spatiotemporal pattern of *bcd* mRNA translation**
203 How does translation of *bcd* vary during embryogenesis? We analysed 3D image stacks at
204 different stages of embryo development from n.c. 4 through n.c. 14. Before n.c.9, there was
205 sustained translation of *bcd* in a region near the anterior cortex (Figure 4A). After nuclear
206 migration in n.c. 9, we observed a gradual decrease in translation events and by the end of
207 n.c. 14, translation events were scarcely detected (Figure 4A-B). To test if the efficiency of
208 translation varied at different positions in the embryo, we quantified and compared the intensity
209 of translation events of single *bcd* particles in the anterior and posterior domain. We did not
210 see any clear changes in the translation intensity between these locations (Figure 4C).

211
212 Translation can depend on the location of mRNA within the cytoplasm. In the early *Drosophila*
213 embryo, for example, apical *twist* mRNA has lower translation than basal mRNAs (55). We
214 analysed and compared the translating *bcd* particles above and below the cortical nuclei from
215 n.c. 9 to late n.c.14. We did not see any significant differences in the translation of *bcd* based
216 on their position, however, there appears an enhanced translation of *bcd* localised basally to
217 the nuclei (Figure S5). We also noticed that upon migration, *bcd* localisation at the anterior
218 pole became more dispersed (Figure S6A). The interphase nuclei and their subsequent mitotic
219 divisions appeared to displace *bcd* towards the apical surface (Figure S6B).
220
221 Our *bcdSun10* not only marks the translating nascent Bcd-SunTag but can also generate a
222 long-range, functional gradient. We can directly test different models of Bcd protein production
223 (3, 10, 12, 58) and how this impacts the formation of the Bcd morphogen gradient. We first
224 compared the concentration profiles of *bcd* mRNA and the protein distribution in our *bcdSun10*
225 line from n.c. 1-8 (prior to cortical nuclear migration), n.c. 9-13 (post cortical nuclear migration),
226 and during n.c.14 (leading up to cellularisation) (Figure 5A). We noticed an overall spread of
227 BcdSun10 beyond the *bcd* signal, consistent with an SDD-like model for gradient formation
228 (Figure 5B-D). The extent of *bcd* mRNA was localised to the anterior in the early embryo, with
229 some dispersal post cortical nuclear migration (Figure 5C). However, there was no apparent
230 long-ranged *bcd* mRNA gradient. For BcdSun10, the early protein gradient was steeper than
231 later in the blastoderm, and always with further extent than the *bcd* mRNA distribution (Figure
232 5D). We saw a reduction of Bcd intensity in n.c. 14, consistent with previous reports (Figure
233 5E) (77).
234
235 Overall, we observe a steady shift in the domain of *bcd* mRNA translation, which correlates
236 with nuclei movements. However, this shift does not result in substantially more dispersed *bcd*
237 translation along the AP-axis. More than 98% of all translation events occurred within 75μm
238 of the anterior pole, regardless of the nuclear cycle. These results support a model of localised
239 Bcd production, restricted to a domain near the anterior pole.
240
241 ***bcd* mRNA degradation in n.c. 14 embryos**
242 We showed a significant reduction in *bcd* mRNA translation from n.c. 13 onwards, and smFISH
243 confirms that during n.c. 14 *bcd* is degraded (Figure 6A-C) (12, 78). Previous work has shown
244 mRNA co-localisation with embryonic P bodies is correlated with degradation (79-81). We next
245 tested if *bcd* was targeted for degradation in embryonic P bodies. We observed *bcd* and
246 Me31B at early, mid, and late n.c. 14 (Figure 6A'-C'). With smFISH, we showed that *bcd* was

evenly distribution on both the apical and basal sides of the nuclei. Co-localisation analysis revealed that *bcd* is not in P bodies at early n.c. 14 (Figure 6A', D).

At mid n.c. 14, *bcd* was localised to the apical side of the nuclei (12). We found that it co-localised with embryonic P bodies, which were also enriched on the apical side (Figure 6B', E-F). As the embryo transitioned into gastrulation, we observed a significant loss of *bcd* while embryonic P bodies remained (Figure 6C'-E-F). Together, this supports a model where, as the embryo transitions to zygotic control, maternal mRNAs in the embryo gather in embryonic condensates for degradation (79-81).

Adapted SDD model of Bcd protein gradient formation

Formation of the Bcd morphogen gradient has been extensively modelled (11, 15, 82). Previous models typically considered the rate of Bcd production stayed constant during early embryogenesis. We then asked if considering the spatiotemporal pattern of *bcd* translation in the SDD model matched the observed Bcd gradient.

We considered the concentrations of *bcd* mRNA, shown as *[bcd]*, and the protein *[Bcd],* where the concentrations are functions of space and time, within a modified SDD model (Figure 7A):

$$\frac{\partial[bcd]}{\partial t} = -\alpha(t)[bcd] \qquad \text{(Eq. 1a)}$$

$$\frac{\partial[Bcd]}{\partial t} = \frac{\partial}{\partial x}\left[D(x)\cdot\frac{\partial[Bcd]}{\partial x}\right] - \mu[Bcd] + \beta[bcd] \qquad \text{(Eq.1b)}$$

We defined time t = 0 to denote egg activation. The initial conditions for [*bcd]* and [Bcd] were given by:

$$[bcd](t=0,x) = f(x) \qquad \text{(Eq. 2a)}$$

$$[Bcd](t=0,x) = 0 \qquad \text{(Eq. 2b)}$$

bcd mRNA was localised in the anterior pole with a form denoted by *f(x)*, (Eq. 2a), shown in Figure 7B(i). We incorporated a delay initially in translation to account for egg activation (Figure 7B(ii)). The rate of *bcd* degradation $\alpha(t)$ increased markedly in n.c. 14 (Figure 7B(iii)).

It was recently observed that the effective diffusivity of Bcd protein varies between the anterior and posterior pole (49). We included this through spatial variation in the diffusion coefficient *D(x)* (Figure 7B(iv)). We assumed that the rate of *bcd* translation after egg activation (β) and Bcd degradation (μ) remained constant. The degradation rate for Bcd has been calculated previously based on protein lifetime measurements (10).

Our modified one-dimensional SDD model generated an exponential-like gradient of Bcd in n.c. 13 (Figure 7C-C'). We emphasise that all the parameters in this model are constrained by experimental measurement, except for β, so it is not over parameterised (Table S5). We found a decay length of around 85-95 μm, consistent with experimental measurements (7, 10, 58). By including more realistic *bcd* mRNA translation, the overall behaviour of the Bcd protein gradient (Figure 7D-D') is consistent with previous observations (58) and our quantification presented here.

Discussion

We have provided a quantitative dissection of when and where *bcd* mRNA is translated in early *Drosophila* development. Translation is restricted until after egg activation by localisation within P bodies. Translation occurs in the anterior pole of the embryo and undergoes a marked decrease after n.c. 12. As embryogenesis continues, *bcd* becomes localised to the apical domain and is degraded, particularly at mid n.c. 14. This rapid degradation of *bcd* correlates with its localisation to P bodies during embryo cellularisation. These observations, along with recent quantifications of Bcd dynamics (49), support a modified SDD model of gradient formation.

In early embryos, Bcd protein is only observed in the anterior pole. This closely matches the *bcd* translation pattern. No significant translation was observed more than 50μm from the embryo anterior. These results argue that *bcd* translation does not occur in the oocyte and against a model of long-ranged protein gradient formation by a dispersed zone of production. Another model suggests that *bcd* is distributed through the embryo and hence can generate a long-ranged Bcd gradient without the need for diffusive transport (12, 83, 84). However, we observe most translation events occurred within 50 μm of the embryo anterior pole. Consistent with previous reports (58), we posit this is due to *bcd* localisation in the anterior region, rather than there being translational regulation of *bcd* in more posterior regions. This means that any graded form of *bcd* translation mostly happens in the anterior and that a long-ranged *bcd* translation gradient does not determine the Bcd protein gradient.

We noticed distinct differences in the apical-basal localisation of *bcd,* especially after nuclear migration to the embryo cortex. This change in apical-basal distribution correlates with a reduction in the observed *bcd* translation. However, it still needs to be tested if the localisation of *bcd* impacts its translation rate. The localisation of mRNAs within the microenvironment defined by each nuclear domain can impact translation in n.c. 14 (55), though whether a similar effect occurs earlier in development is unclear.

319 The rapid loss of *bcd* at n.c. 14 has been previously quantified (58) and here we discovered it
320 also correlates tightly with localisation to P bodies (Figure 6). It remains unclear what
321 determines the model of *bcd* degradation at n.c. 14, and if it is due to global degradation of
322 maternal mRNA or a specific regulation of *bcd* mRNA (44). Testing for *bcd* degradation is
323 challenging. One method is to infer degradation by examining spectral signal with different
324 smFISH probes for the 5' and 3' UTRs (81, 85). However, the *bcd* 5' UTR is very short, and
325 we were unable to make effective probes. An alternative approach is to target the *bcd*
326 instability element (BIE). This regulates degradation of *bcd* (78) and is located within the more
327 accessible 3' UTR.
328
329 It will be interesting to explore how differences in P bodies between the oocyte and embryo
330 affects mRNA. P bodies appear to switch function, from shielding *bcd* from translation to
331 enhancing *bcd* degradation. Prior to cellularisation, we found that Me31B condensates were
332 insensitive to cycloheximide. However, after cellularisation begins, they become sensitised to
333 cycloheximide (86), suggesting a change in their structure. A similar change in RNP function
334 has been shown in *Drosophila* germ granules (87). Germ granules transition from protecting
335 their mRNA contents to targeted degradation of specific mRNAs after germ cell specification.
336 This is accomplished through recruitment of degradation factors as the granules grow through
337 fusion. Decapping activity in these enlarged, functionally different germ granules lead the
338 authors to call them P body-like. It is intriguing to consider that many RNP granules in
339 *Drosophila*, and more broadly in *C. elegans, Xenopus*, zebrafish, will likely undergo changes
340 in size, composition, and function throughout development. Relatedly, due to the conserved
341 nature and wide-ranging downstream effects, it is intriguing to consider the possibility that
342 Endos is a condensate regulator both within *Drosophila* eggs as well as more generally.
343
344 Over 40 years of work span from the original proposition of the SDD model for Bcd protein
345 gradient formation. Here, we quantitatively assay the production of Bcd *in vivo*, which is
346 arguably the last piece required to understand Bcd gradient formation. We see that the original
347 SDD model, which assumed that dynamic parameters such as production rate and diffusion
348 were constant in space and time, was too simple. However, with suitable modifications, like
349 spatially varying diffusion and temporally altering translation, it can explain the formation of
350 the Bcd gradient.

Contributions:

Project conception: ML, TES, TTW. Experimental design: TA, ELW, ML, TES, TTW. Experiments: TA and ELW with support from XS, PB, MV and ML. Analysis: TA, ELW, XS with support from AT, TES and TTW. Modelling: TES. Writing: TA, ML, XS, TES, ELW, TTW with all authors contributing to final version. Funding acquisition: ML, TES, TTW.

Acknowledgements

We are very grateful to members of the Lagha, Saunders and Weil labs for support and comments on the project. We thank Jeremy Dufourt for advice on initial strategy for using Suntag with Bicoid and sharing plasmids (55). ML funding: ERC lightRNA2Prot, Marie Sklodowska-Curie Actions and CNRS. TES thanks core funding from the Mechanobiology Institute, Singapore and startup funding from Warwick Medical School. TTW thanks the Wellcome Trust Institutional Strategic Support Fund, University of Cambridge (grant number 097814) and Biotechnology and Biological Sciences Research Council Doctoral Training Partnerships studentship (ELW). ML acknowledges the Montpellier Resources Imaging facility (France-BioImaging) and the Drosophila facility (Biocampus). The lab of ML is funded by grants from the Fondation Bettencourt Schueller, the European Molecular Biology Organization Young Investigator program (EMBO YIP). The funders had no role in study design, data collection and analysis, decision to publish, or preparation of the manuscript.

Methods

Generation of SunTag *bcd* transgenic fly lines

bcdSun32 was generated by replacing N-terminal eGFP of eGFP:Bcd-pCaSpeR4 construct (kindly gifted by Thomas Gregor (7)) by 32xSunTag repeats (kindly gifted by Mounia Lagha (55)). The 32xSunTag fragments are flanked by NheI and SpeI restriction sites at their N and C-terminal ends respectively by PCR, and then ligated into the eGFP:Bcd construct, replacing eGFP. Likewise, the first 10xSunTag repeats of 32xSunTag were ligated in the same way to generate *bcdSun10* construct (Figure S2A). Both Bcd SunTag constructs from the donor pCaSpeR4 construct were recombined into w+attB construct (addgene 30326) and flies were generated by phiC31 recombination into attP40 site of chromosome 2. The injection and generation of fly lines were done by BestGene Inc. USA.

The *bcdSun10* fly lines were crossed to the *bcd* null allele mutant, bcd^{E1}. *bcdSun10*;bcd^{E1} fly lines were viable, suggesting our construct can, at least partially, complement the function of endogenous Bcd. smFISH was carried out to test if *bcdSun10*;bcd^{E1} effectively replaced the function of endogenous Bcd in the blastoderm. Stellaris smFISH probes with distinct fluorophores were used for SunTag and *bcd* coding regions of the *bcdSun10* mRNA. This

388 enabled us to confirm that the only contribution of maternal *bcd* mRNA was from our *bcdSun10*
389 in the bcd^{E1} background (Figure S2). Co-localisation analysis in the early blastoderm revealed
390 ~90% of the mRNA were accounted for *bcdSun10* (Figure S2B). Further, the immunostaining
391 of the blastoderm embryos with anti-GCN4 antibody revealed the translocation of the
392 *bcdSun10* into the nuclei, unlike *bcdSun32*, eventually forming an anterior posterior gradient
393 similar to endogenous Bcd (Figure S2C-E).
394
395 **Preparation of oocytes**
396 Twenty female flies and ten male flies of the correct genotype were transferred into a vial
397 containing fly food supplemented with yeast and were incubated at 25°C for forty-eight hours
398 before dissection (88).
399
400 **Oocyte dissection**
401 Fattened or aged female flies were anaesthetised, and the posterior tip of the abdomen was
402 removed using a set of fine forceps. The ovaries were then removed from the open posterior
403 end by squeezing the abdomen (88).
404
405 **Fly husbandry and preparation of embryos**
406 Fly stocks were maintained at 21°C in vials that contained standard cornmeal starch agar fly
407 food. To collect flies for experimentation or for genetic crosses, twenty females (virgin females
408 were used for genetic crosses) and ten males were transferred into a plastic bottle containing
409 yeasted cornmeal starch agar fly food at 25°C. Either virgin females or males from this
410 generation were used for additional genetic crosses, or females younger than 10 days old
411 were selected for experimentation. Collected embryos were dechorionated in 50% bleach for
412 2 minutes before excess bleach was removed with distilled water.
413
414 **Chemical and pharmacological treatments of oocytes**
415 Hexanediol and sodium chloride: Dissected oocytes were incubated for 20 minutes in 5% 1,6-
416 HD, 5% 2,5-HD, or 400 mM NaCl before immediate fixation. As controls, dissected oocytes
417 were incubated in PBS or SIM for equal amounts of time before fixation.
418
419 *in vitro* activation of stage 14 oocytes (fixed): Dissected stage 14 oocytes were incubated in
420 activation buffer (AB), for 30 minutes at room temperature. Activated oocytes were incubated
421 in SIM for 0-30 minutes. To ensure that only activated oocytes were visualised, oocytes were
422 treated with 50% bleach for two minutes. The activated oocytes were then fixed using the
423 embryo fixation method. As a control, oocytes were incubated in SIM for the same time period.
424

425 Drugs that inhibit the calcium wave: Dissected stage 14 oocytes were incubated in SIM that
426 contained NS8593 for 30 minutes. The oocytes were then activated in vitro following the same
427 steps as above, with all solutions containing the pre-incubation drug. As a control, oocytes
428 were incubated in SIM (with no AB step) with the drug. Additionally, oocytes were incubated
429 in SIM, followed by AB, followed by SIM with a 1:1000 dilution of either DMSO or ethanol.
430
431 **Fixation**
432 Oocytes were incubated 1 ml of 4% paraformaldehyde for 15 minutes before immediate
433 washing with 0.1% PBST (89). 10-20 pairs of ovaries were dissected and transferred to room-
434 temperature Schneider's Insect Medium (SIM). Ovaries were teased apart using dissecting
435 probes until single ovarioles and oocytes were released.
436
437 Embryos were transferred into an Eppendorf tube that contains equal parts paraformaldehyde
438 and heptane for 15-30 minutes, depending on the probes or antibodies used, before the
439 paraformaldehyde phase was removed and replaced with 100% methanol. The sample was
440 then shaken vigorously before all the solution was removed. Embryos were then rinsed with
441 methanol and/or ethanol before being washed in 0.1% PBST (89).
442
443 **Single molecule fluorescence *in situ* hybridisation (smFISH)**
444 Probe design: Custom 20 nucleotide Stellaris FISH Probes were designed against the 3' UTR
445 of *bcd,* coding region of *bcd*, and 32x SunTag by utilising the Stellaris RNA FISH Probe
446 Designer and were the same as designed in (65) (Biosearch Technologies, Inc
447 - www.biosearchtech.com/stellarisdesigner). 32x SunTag and *bcd* 3'UTR Probes were
448 labelled with Quasar 570 and endogenous *bcd* is labelled with Quasar 670 were ordered for
449 smFISH from Biosearch Technologies, Inc (Tables S2-4).
450
451 Buffers: Wash buffer was created by mixing the commercially available 'Wash Buffer A', de-
452 ionised formamide and nuclease free water in a 2:1:7 ratio or was made using 2% sodium
453 citrate buffer (SSC)+10% formamide. Hybridisation Buffer was created by mixing 'Stellaris
454 Hybridisation Buffer' with de-ionised formamide in a 9:1 ratio.
455
456 Hybridisation: The hybridisation protocol was adapted from (55, 58). Briefly, fixed oocytes or
457 embryos were permeabilised with 0.2% triton X-100 and washed in PBST. When necessary,
458 embryos were blocked in PBST+RNase inhibitor+0.5% ultrapure BSA for 45 mins, before
459 being washed in a 'wash buffer' solution. The samples were then pre-incubated in
460 hybridisation buffer for two hours at 37°C. The hybridisation buffer was removed and replaced
461 by the hybridisation buffer with smFISH probes for overnight incubation at 37°C, when using

462 anti-GCN4 antibodies in conjunction with smFISH, primary antibodies were incubated
463 overnight in the hybridisation buffer (90). The samples were then washed in hybridisation
464 buffer before repeated washes in prewarmed wash buffer, when using anti-GCN4 antibodies
465 in conjunction with smFISH, secondary antibodies were incubated with the final wash buffer
466 wash, before being washed in 2X SSC. Finally, all samples were washed multiple times in
467 0.1% PBST.
468
469 Immunostaining: Nanobody labelling on oocytes or embryos, samples were blocked in a 4%
470 BSA solution and then incubated with nanobodies, either GFP booster or RFP booster, in
471 0.1% PBST for one hour at room temperature. For anti-GCN4 immunostaining not in
472 conjunction with smFISH, samples were incubated for two hours with the primary antibody,
473 followed by washing with 0.1% PBST and incubation with the secondary antibody for two
474 hours. After incubation, all samples were washed with 0.1% PBST.
475
476 Washed samples were transferred to a microscope slide and positioned using a dissecting
477 probe. Excess PBST was removed before a single drop of Slowfade Diamond with DAPI or
478 Prolong Diamond with antifade was added to the sample. A 22 x 22 mm coverslip was lowered
479 onto the sample, and the coverslip was sealed with nail varnish and laid flat in the dark for 24
480 hours before imaging.
481
482 Imaging: All oocyte imaging was completed on an Olympus FV3000 inverted confocal
483 microscope. Embryo imaging was performed on Olympus FV3000 or Olympus Spinning Disc
484 systems. All images were taken using silicone oil 30x (0.95 NA) or 60x (1.4 NA) objectives. A
485 region of interest was placed around either a whole single oocyte or embryo (30x objective)
486 or a specific region of the oocyte or embryo (60x objective), Images were taken at a resolution
487 of 1024 by 1024, or 2048 by 2048 pixels. 405, 488, 561 and 640 nm lasers were used. Laser
488 power was adjusted to ensure that there was a full range of grey values and that the saturation
489 of pixels was limited.
490
491 The images for the quantification of *bcd* foci in the embryo and their co-localisation to
492 translating SunTag, were acquired on an Olympus FV3000 confocal microscope with the
493 following conditions: 60x magnification, 4x zoom, 2 line averaging, slice thickness of 0.4 µm.
494 The regions of high, moderate, and low dense *bcd* foci from the anterior domain and a very
495 low *bcd* region in the posterior were imaged for a total thickness of 10-15 µm.
496
497 Fixed Imaging: Optimised step-size Z-stacks of fixed egg and embryos were collected; all Z-
498 stacks were started at the cortex and extended 10-15 µm into the oocyte or embryo. For co-

localisation studies, smFISH, and SunTag translation assays, where maximum resolution was imperative. Imaging parameters were optimised to improve resolution: 60 x objective used; pinhole: 1 airy unit; scan speed – 400 Hz; 2x line averaging; 2048 by 2048 pixels; and optimised Z-step (300 nm) (56).

Image Analysis

Translation quantification: High-resolution image stacks were segmented to identify specific *bcd* foci. We used the trainable Weka segmentation plugin of ImageJ to train and classify the *bcd* foci. A classifier model created from a single image slice was applied to the Z-stack, thus classifying the *bcd* through the whole stack. The segmented particles were analysed using the Fiji particle analysis plugin that provided information on the size, shape, intensity and counts of all particles. The crowded particles that failed to segment properly, which was often the case within highly dense *bcd* regions, were not considered. We also excluded foci with low brightness. The segmented ROIs of *bcd* foci were applied to the anti-GCN4 channel. The mean intensities from anti-GCN4 channel were background corrected, and the positive mean values provided the number of co-localising SunTag to *bcd* particles *i.e.,* these particles were translating *bcd*. The plots were made in Graphpad Prism 8.0.

When automated methods were not accurate for detecting partial co-localisation (91), manual analyses were undertaken on images with only partial co-localisation. Images for both channels were thresholded, then an overlay of the threshold outline for channel one (*bcd*) was projected onto the channel two image (anti-GCN4). The number of particles in *bcd* channel that overlapped particles in anti-GCN4 channel was counted, and *vice versa*. To ensure that this partial co-localisation was not due to chance, images of one channel were inverted and the analysis was completed again.

Statistical Analysis

n numbers: 10 to 20 females or 30 embryos (biological repeats) were used for each experiment and a global overview of the experimental results was acquired by visualising 20-30 oocytes or 30 embryos for each experimental condition unless stated otherwise. A smaller number of representative oocytes were subjected to high resolution imaging and analysis as described above. The “n” used in figures represents independent oocyte or embryo samples.

All statistical analyses were performed in R. For all statistical analyses, asterisks represent the following n.s. not significant * $P<0.05$, ** $P<0.01$, *** $P<0.001$.

535 Continuous data: Tests for normality were completed before proceeding with the appropriate
536 parametric or non-parametric test. For comparison between two groups, an unpaired student
537 t-test (STT) or a Wilcoxon signed-rank test (WSRT) was used.
538
539 Categoric data: A χ^2 test (CST) or Fisher's exact test (FET) was used to determine if there
540 were significant differences between groups. This depended on sample size Fisher's exact
541 test is preferred for small sample sizes (<50).
542
543 **Fly lines**
544 Table S1 in the Supplementary Information outlines all lines used in this study.
545
546 **Reagents**
547 Summary of reagents and tools used in this work

Reagent	Supplier/ provider	Catalogue number	Concentration used
Antibodies			
GFP Booster Alexa 488	Chromotek	gb2AF488-100	1:1000 in 0.1% PBST
Rabbit GCN4 Antibody (C11L34) - Chimeric	Novus Biologicals	NBP2-81274SS	1:200 in 0.1% PBST
Goat anti-Rabbit Cy3	Thermofisher Scientific	A10520	1:200 in 0.1% PBST
Goat anti-Rabbit Alexa Flour 647	Thermofisher Scientific	A21245	
Buffers, chemicals, and pharmacological treatments			
Schneider's Insect Media (SIM)	Gibco	21720024	1 X
Activation Buffer (AB)	Made in house: 3.3 mM NaH_2PO_4, 16.6 mM KH_2PO_4, 10mM NaCl, 50 mM KCl, 5% polyethylene glycol (PEG) 8000, 2mM $CaCl_2$, brought to pH 6.4 with a 1:5 ratio of NaOH:KOH (260 mOsm) (Mahowald, Goralski and Caulton, 1983)	-	1 X
Dulbecco's Phosphate Buffered Saline (without $CaCl_2$)	Sigma Aldrich	D8537	1X
1,6 Hexeandiol (1,6-HD)	Sigma Aldrich	240117	5% in Schneider's Insect Medium or 1x PBS
2,5 Hexeandiol (2,5-HD)	Sigma Aldrich	H11904	5% in Schneider's Insect Medium or 1x PBS
Sodium Chloride (NaCl)	Sigma Aldrich	S9888	400 mM in H_2O
NS8593	Sigma Aldrich	492031	Stock: 100 mM in ethanol Final concentration: 100 µM in Schneiders Insect Medium or Activation Buffer (92)

Household Bleach	ESPO	200-300-0011/1	50% in H_2O
Paraformaldehyde	Thermofisher Scientific	J19943-K2	4% in PBS
Methanol	32213	Sigma Aldrich	1 x
Heptane	Thermofisher Scientific	H/0106/PB17	1 x
Triton™ X-100	Sigma Aldrich	X100	0.2% in PBS
Polyoxyethylenesorbitan Monolaurate (Tween-20)	Sigma Aldrich	P1379	0.1% in PBS
De-ionised Formamide	Sigma Aldrich	S4117	10%-30% in various FISH buffer solutions
20 X SCC	Sigma Aldrich	S6639	2X-5X SCC in various FISH buffer solutions
Dextran sulphate	Sigma Aldrich	D6001	10% in various FISH buffer solution
'Wash Buffer A' for Stellaris smFISH	LG Biosearch Technologies	Cat# SMF-WA1-60	20% in de-ionised Formamide and nuclease free H_2O
'Hybridisation Buffer' for Stellaris smFISH	LG Biosearch Technologies	Cat# SMF-HB1-10	90% with de-ionised Formamide
Hybridisation buffer for ImmunoFISH	Made in house (10% Formamide, 2xSSC, Ecoli tRNA (0.36mg/ml), VRC (2mM), 5% Dextran sulphate, ultra pure BSA(0.25mg/ml), stellaris probes, Primary antibody (1:500)		
Tris EDTA (TE) Buffer	Made in house (10 mM Tris-HCl, 1 mM EDTA, pH 8.0)	-	1 x
Slowfade Diamond Antifade Mountant with DAPI	Thermofisher Scientific	S36934	1 X
Oligonucleotides			
(1) Custom Stellaris FISH Probes for the 3'UTR of *bcd* RNA labelled with a Quasar 570 (2) Bcd coding region Quasar 670 (3) 32xSunTag Quasar 570	Stellaris	(See table 2.3 for list of smFISH probes)	Stock: 12.5 μM in TE buffer Final Concentration: 50 nM in 0.25 ml Hybridization buffer
Software and Algorithms			
Image J	Schneider et al., 2012	https://imagej.nih.gov/ij/	
R Studio/ R Software	R Studio Team 2024	http://www.rstudio.com/	
Graphpad Prism			
Other			
Standard Cornmeal Starch Agar FlyFood	Made in house by the Fly Facility, Department of Genetics, University of Cambridge	N/A	N/A
Olympus FV3000 Confocal Laser Scanning Microscope	Olympus	FV3000	N/A

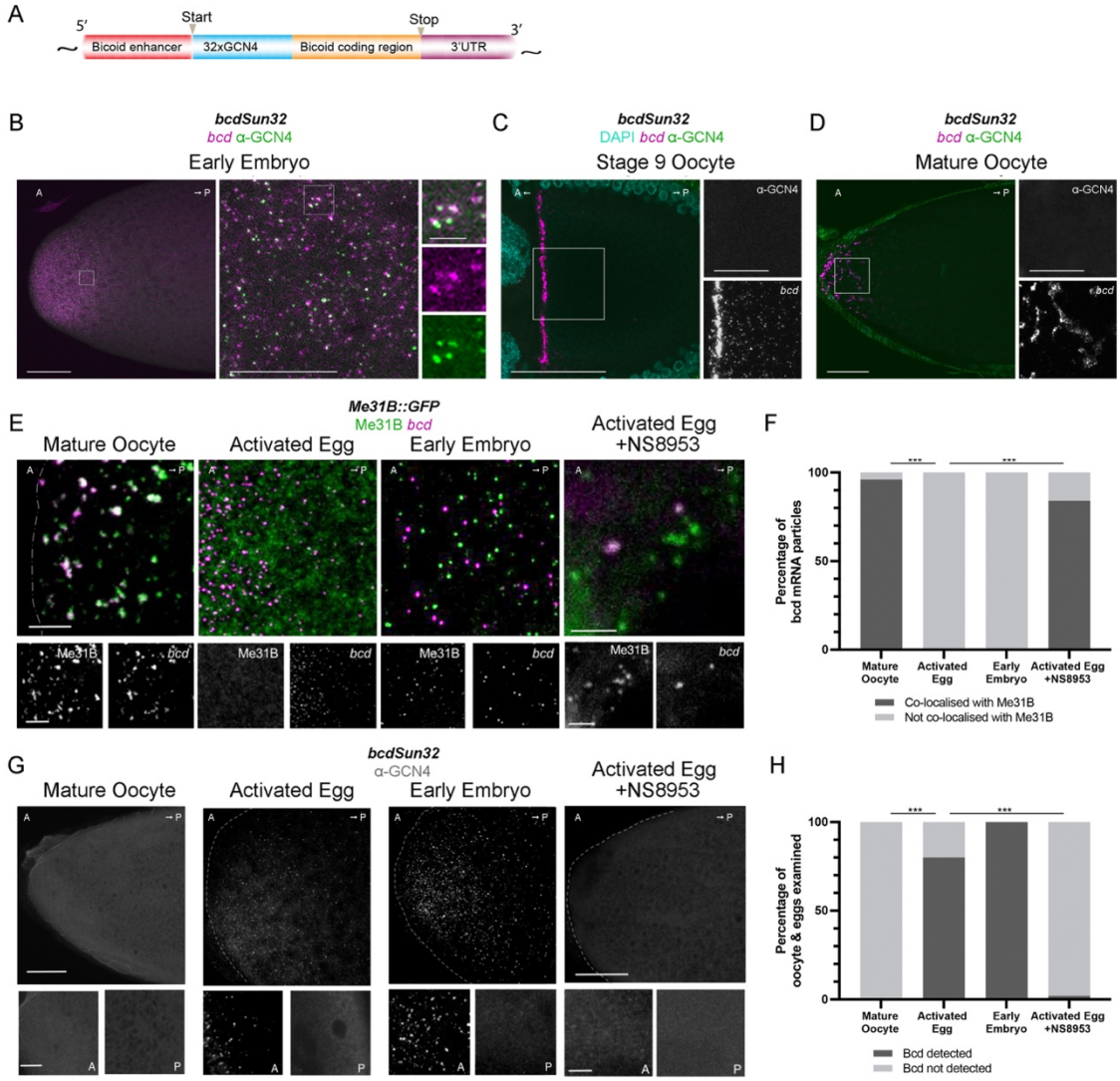

Figure 1: *bcdSun32* reporter enables visualisation of *bcd* mRNA translation

A: Schematic illustrating the insertion of 32x SunTag repeats at the N-terminal of the *bcd* coding region after the start codon.

B: Representative image of *bcdSun32* in the early embryo (from 15 samples) with *bcd* translation detected by immunostaining for GCN4 (green) and *bcd* mRNA (magenta). Boxed region magnified on right. Boxed region on right further magnified. N = 20. Scale bars: left 50 µm; middle 10 µm; right 3 µm.

C-D: Representative fixed 5-10 µm Z-stack images showing *bcdSun32* labelled *bcd* (magenta, smFISH) localising to the anterior margin of stage 9 and 14 (mature) oocytes. SunTag labelled Bcd protein (green, anti-GCN4) is not detected in stage 9 or 14 oocytes. N = 20. Scale bars: 50 µm; zoom 10 µm.

E: Representative fixed 10 µm Z-stack images (from 10 samples) showing Me31B::GFP (green, anti-GFP-nanobody) and *bcd* (magenta, smFISH) at the anterior in mature oocyte, *in vitro* activated egg, early embryo 30-minute post fertilisation, and *in vitro* activated egg

incubated with NS8953, a calcium channel blocker. Single channel images are shown for Me31B and *bcd*. Scale bar: 5 μm.

F: Quantification of the co-localisation (as shown in E) between *bcd* particles and Me31B::GFP particles. N = 6 for mature oocytes, *in vitro* activated egg, early embryos. N = 3 for *in vitro* activated egg incubated with NS8953 due to difficulty with particle detection post oocyte swelling.

G: Representative fixed 10 μm Z-stack images (from 10 samples) showing BcdSun32 protein (anti-GCN4) at the anterior of a mature oocyte, *in vitro* activated egg, early embryo 30-minute post fertilisation, and *in vitro* activated egg incubated with NS8953. Zoomed images of the mature oocyte show that Bcd protein is not detected at the anterior posterior pole of the same mature oocyte or *in vitro* activated egg incubated with NS8953. However, zoomed images of the *in vitro* activated egg and early embryo 30-minute post fertilisation show that BcdSun32 protein was detected at the anterior and not the posterior pole. Scale bar: 20 μm; zoom 2 μm.

H: Quantification of the number of mature oocytes or early embryos that displayed *bcd* translation as measured by the presence of BcdSun32 protein at the anterior but not the posterior. N = 10 for each condition.

Anterior to the left and posterior to the right in all images.

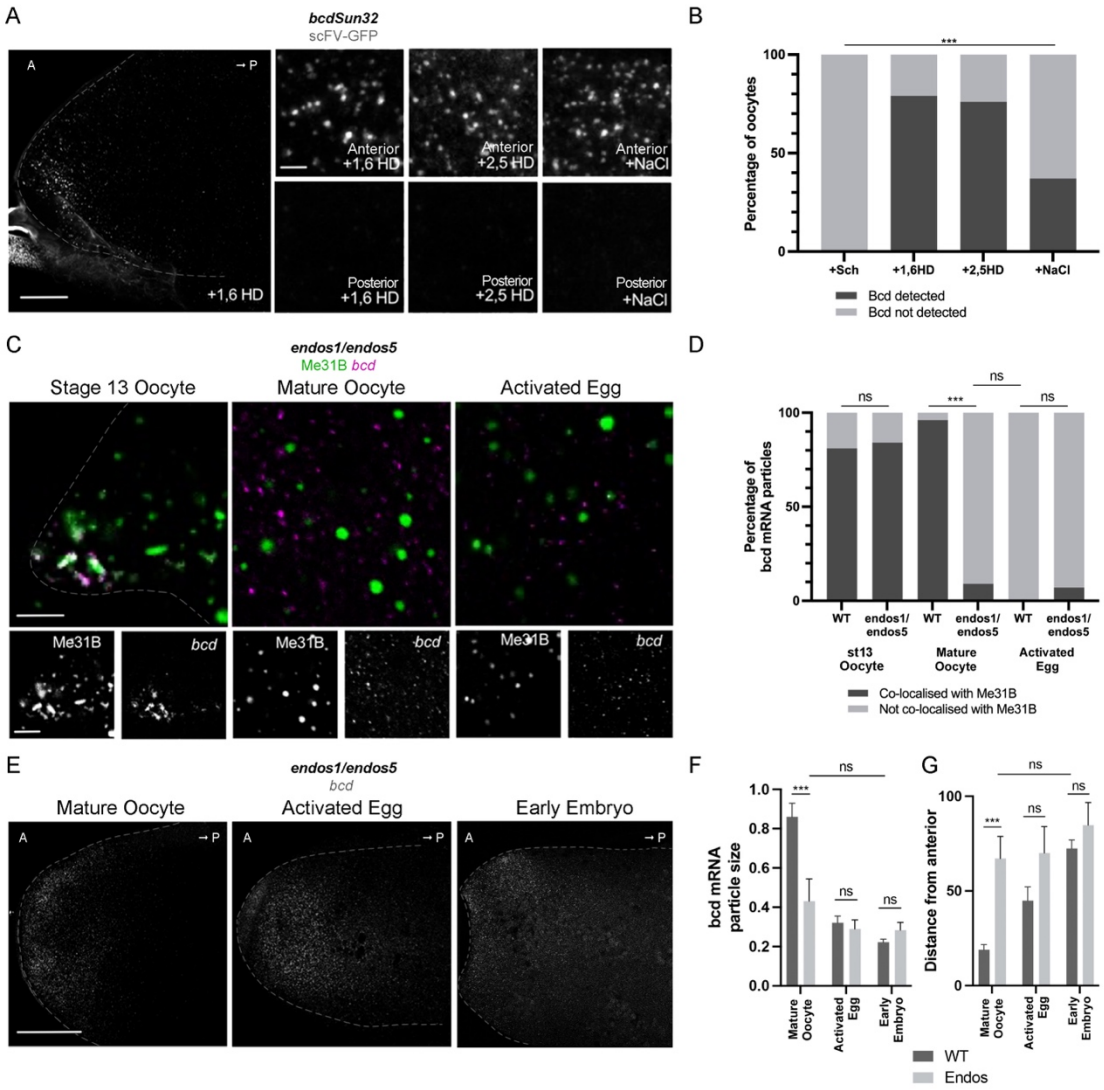

Figure 2: Chemical and genetic manipulation of P bodies can cause *bcd* mRNA misregulation

A: Representative fixed 10 µm Z-stack image (from 10 samples) showing the overall distribution of BcdSun32 protein (scFV-GFP, anti-GFP-nanobody) at the anterior of a stage 14 (mature) oocyte incubated in 5% 1,6 hexanediol for 20 minutes. Zoomed images show that BcdSun32 protein is detected at the anterior pole and not at the posterior pole of the same 5% 1,6 hexanediol, 5% 2,5 hexanediol, and 400 mM NaCl treated mature oocytes. Scale bars: Left 20 µm; right 2 µm.

B: Quantification of experiments shown in A. The number of oocytes that displayed Bcd protein at the anterior as measured by the presence of BcdSun32 at the anterior of the oocyte, but not the posterior. N = 30 oocytes for each treatment. Scale bar: 5 µm.

C: Representative fixed single plane image showing the distribution of Me31B::GFP (green, anti-GFP-nanobody) and *bcd* (magenta, smFISH) in an Endos mutant stage 13 oocyte, mature oocyte, and an *in vitro* activated egg. Scale bar: 5 µm.

D: Quantification of experiments shown in C. Colocalisation is shown between *bcd* and Me31B in both wildtype and mutant stage 13 oocytes and in wildtype stage 14 oocytes. Significantly less, or no colocalisation is detected in mutant stage 14 oocytes or both wildtype and mutant activated eggs. N = between 6-10 oocytes for each genotype.

E: Representative fixed 10 µm Z-stack image showing the overall distribution of *bcd* (smFISH) in an Endos mutant background at the anterior of the mature oocyte, *in vitro* activated egg, and early embryo. *bcd* appears to be particulate and diffuse at the anterior pole of all samples. Scale bars: 20 µm.

F: Quantification of experiments shown in E. Quantification of the size of *bcd* particles in Endos mutant background compared to the wildtype in mature oocytes, activated eggs, and early embryos. Particles in wildtype mature oocytes are significantly larger than in Endos mutant backgrounds. Particles in an Endos mutant background all of a similar size and are not significantly different from particles in wildtype activated eggs or early embryos. Wilcoxon signed-rank test, *** $p < 0.001$, N = 5.

G: Quantification of experiments shown in E. Quantification of the distance from the anterior of *bcd* particles in an Endos mutant background compared to the wildtype in mature oocytes, activated eggs, and early embryos. In mature oocytes, particles in an Endos mutant background are significantly further from the anterior than in wildtype. Particle distance from the anterior is not significantly different Endos mutant mature oocytes as compared to wildtype early embryos. Wilcoxon signed-rank test, *** $p < 0.001$, N = 5.

Anterior to the left and posterior to the right in all images.

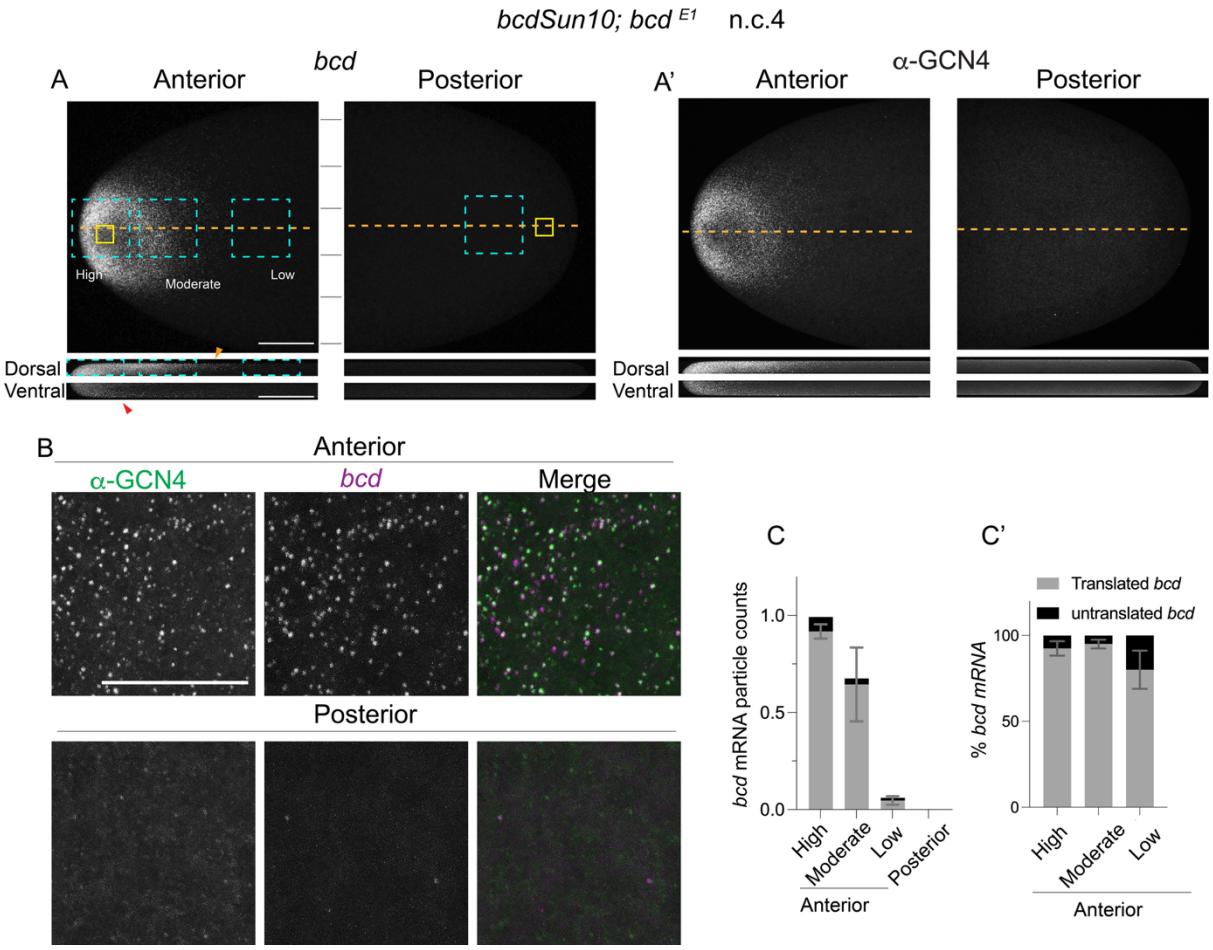

Figure 3: *bcd* mRNA is translated exclusively in the anterior domain of the early *Drosophila* embryo

A-A': Projected Z-stacks of the anterior and posterior domain of n.c. 4 embryo expressing the *bcdSun10* transgene, stained for *bcd* coding region (magenta) and SunTag, anti-GCN4 (green) using Immuno-FISH. The projected cross sections in the bottom panel show the dorsal and ventral surface of the anterior and posterior domains of the embryo. Translating *bcdSun10* is shown in A' along with projected cross sections. Scale Bars: 50 µm.

B: Yellow boxes from A are magnified to show colocalisation of SunTag to *bcd*. Scale Bars: 10 µm

C: Normalised *bcd* counts from the cyan boxes in A located at regions of varied mRNA counts across AP-axis. Data normalised to the total mRNA counts from the most anterior region analysed. N = 3 embryos.

C': Percentage of translated and untranslated *bcd* mRNA at different locations (cyan boxes in A) in the anterior and posterior domains (N = 3 embryos) in n.c. 4. Error bars = s.d.

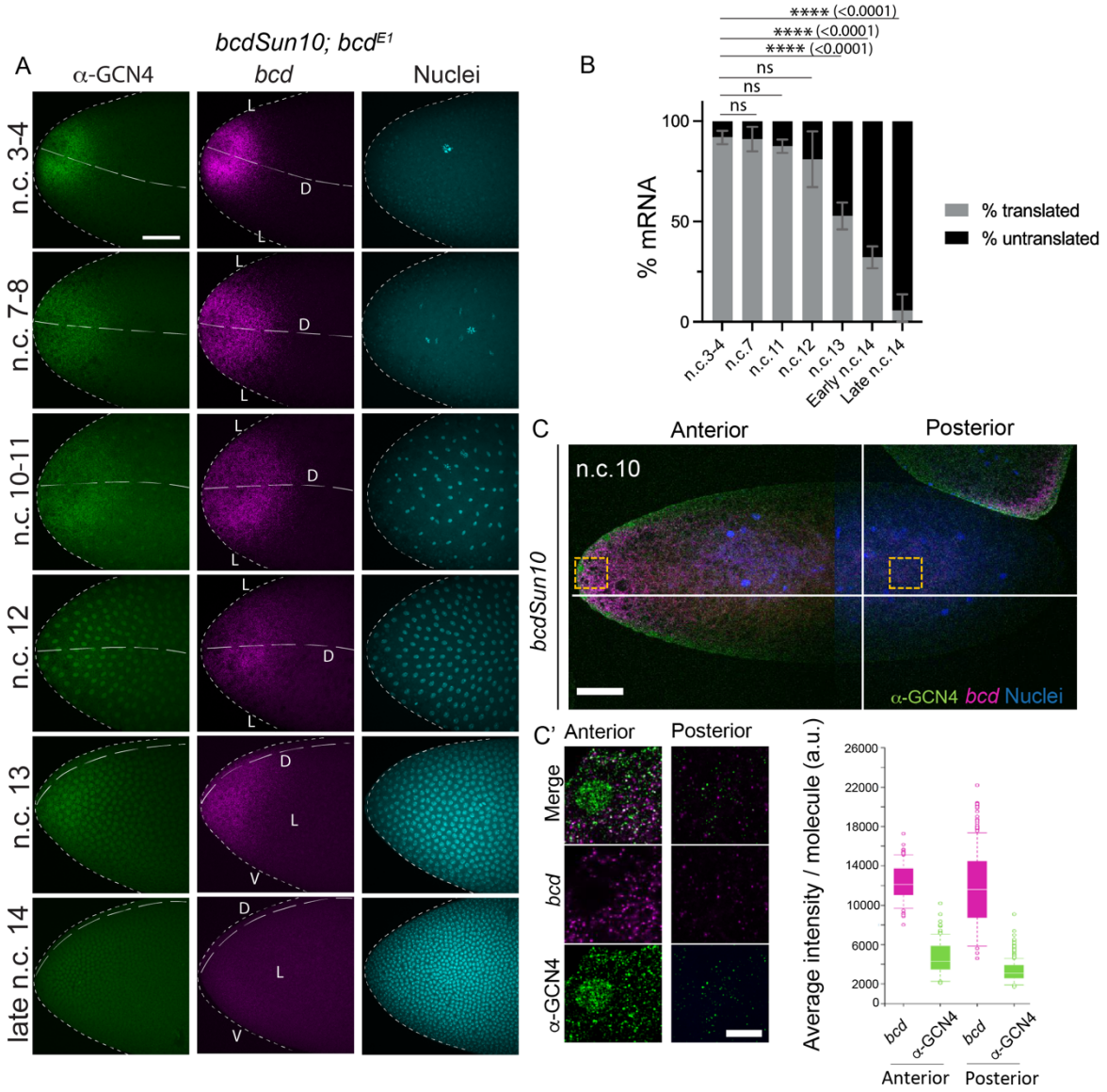

Figure 4: Temporal changes in *bcd* translation from early to late blastoderm

A: *bcdSun10* translation detected through immuno-FISH marked for SunTag translation (anti-GCN4, green) and *bcd* (magenta) from the early to late blastoderm embryo. D = dorsal; V = ventral; V = ventral. Scale bars: 50µm.

B: Percentage of *bcd* undergoing translation at different nuclear cycles. N = 3 embryos in each of the nuclear stages. Error bars = s.d.

C: Projected Z stacks of the anterior and posterior domains embryos expressing *bcdSun10* transgenes. *bcd* reporters and translation spots were detected by Immuno-FISH using *bcd* probes and anti-GCN4 shown in magenta and green respectively. Quantification of the single molecule average intensity for *bcd*-reporters smFISH and GCN4 immunofluorescence signals in anterior and posterior domains (lower right panel), N=3 embryos. Scale bars: C 50 µm; C' 10 µm.

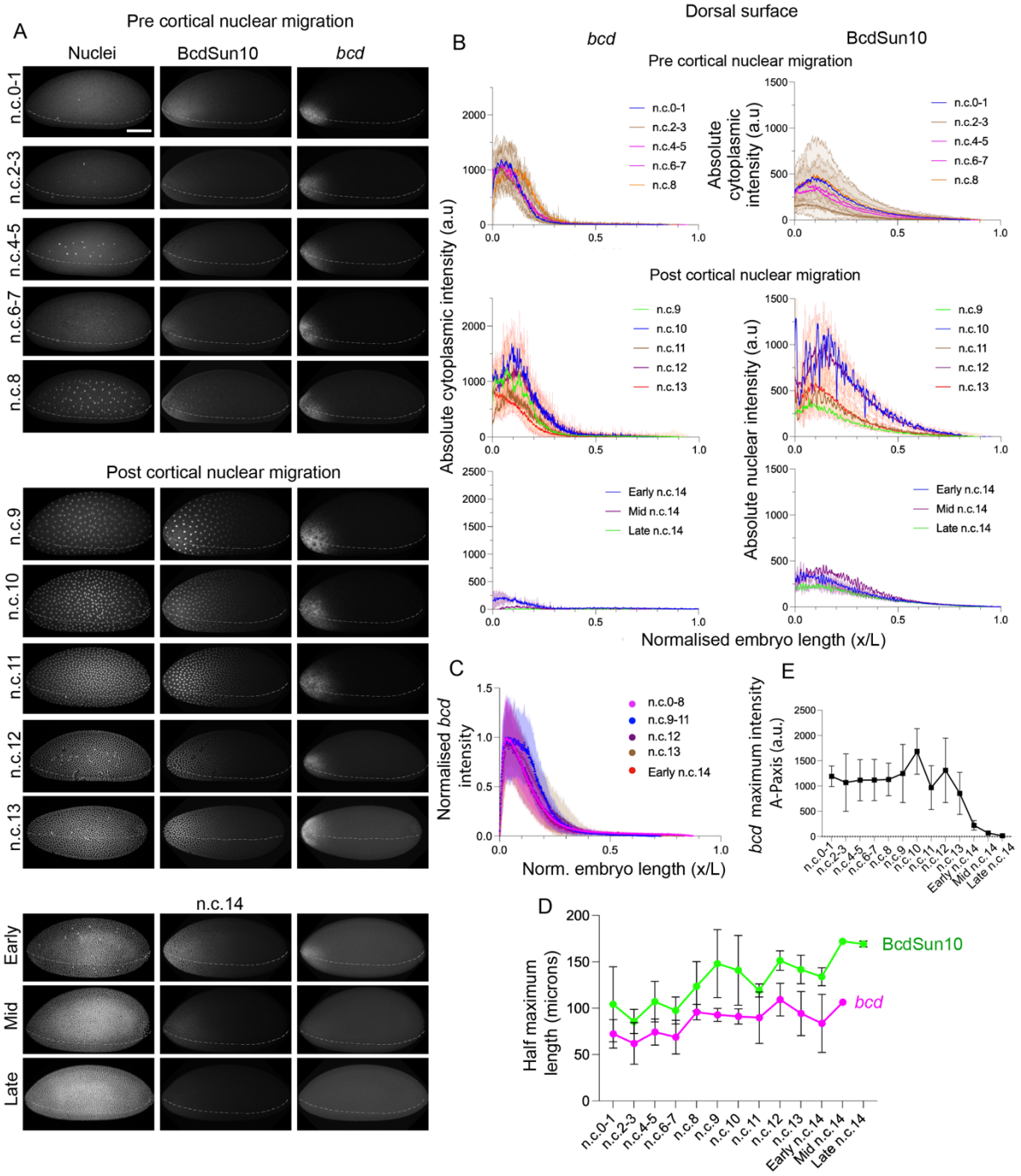

Figure 5: The *bcdSun10* gradient is formed by spread from the translation domain

A: *bcdSun10;bcd^{E1}* embryos at different stages, showing the evolution of the SunTag-Bcd gradient (middle panel) in pre-cortical, post-cortical nuclear migration and n.c.14 with respect to the *bcd* distribution (right panel). The embryos are stained with anti-GCN4 antibody (Bcd-SunTag), *bcd* (mRNA) and DAPI (nuclei). Embryos classified based on the nuclear counts and internuclear distances from the DAPI staining. Broken lines indicate the mid-dorsal lines of the embryo. Scale bar: 50 µm.

B: Line plots showing the intensity of *bcd* (left) and anti-GCN4 (right) measured across the AP-axis of the embryo's mid dorsal surface at different blastoderm stages.

C: Line plot showing the intensity of *bcd* across the AP-axis of the embryo's mid dorsal surface.

D: Distance from anterior pole for *bcd* maximum intensity to decrease by half from peak value in anterior.

E: Maximum intensity *bcd* across cycles.

C-E, embryo numbers: N = 3 (n.c.0-1), N = 4 (n.c.2-3), N = 5 (n.c.4-5), N = 3 (n.c.6-7), N = 3 (n.c.8), N = 3 (n.c.9), N = 3 (n.c.10), N = 2 (n.c.11), N = 4 (n.c.12), N = 6 (n.c.13), N = 2 (Early n.c.14), N = 1 (Mid n.c.14), and N = 2 (Late n.c.14).

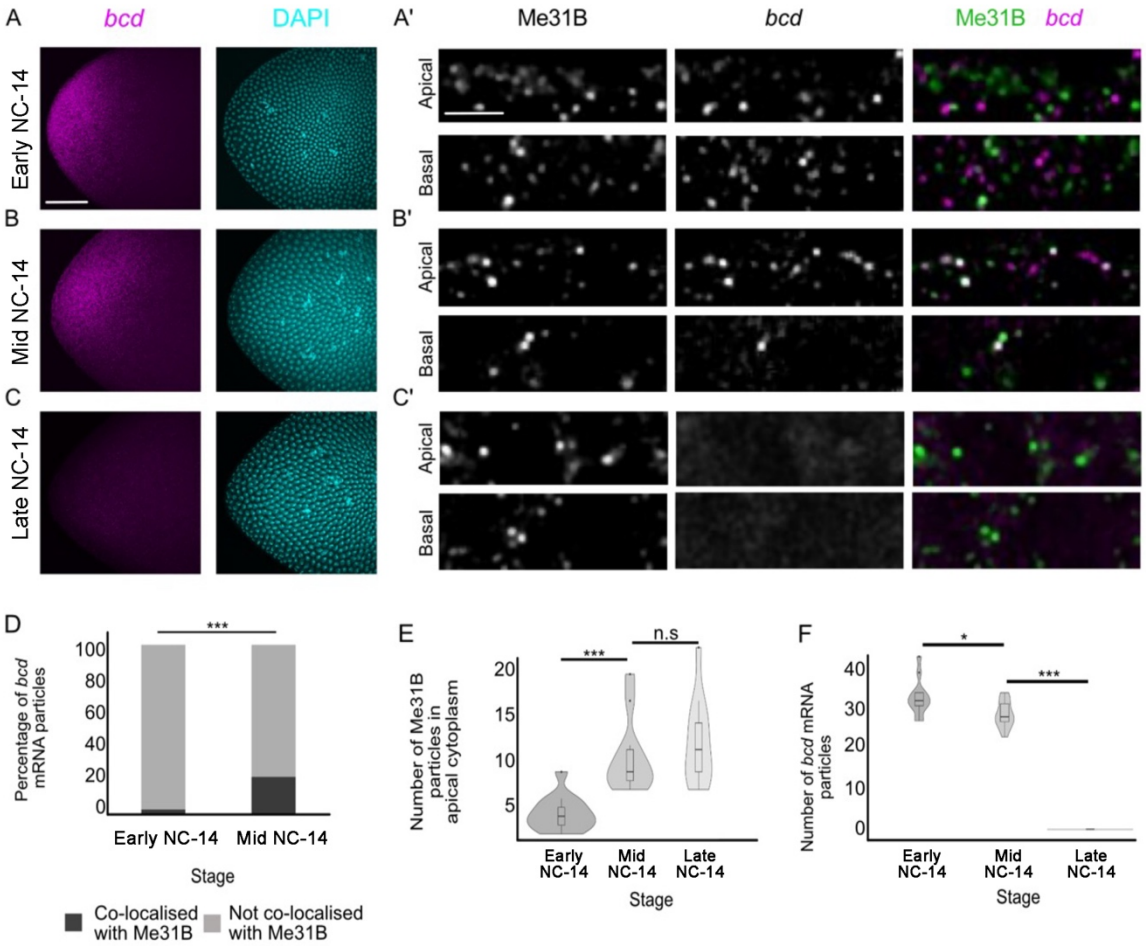

Figure 6: *bcd* re-associates with P bodies in n.c. 14, coinciding with their degradation.

A-C: Representative fixed projected Z-stack images (from 20 embryos) showing *bcd* (magenta, smFISH) and DAPI (cyan) early n.c. 14, mid n.c. 14, and late n.c. 14. Scale bars: 50 µm.

A'-C': Representative fixed single plane images showing the apical side and basal side of early n.c. 14, mid n.c. 14, and late n.c. 14. Me31B::GFP (anti-GFP-nanobody), *bcd* (smFISH), and merge shown. N = 10 embryos. Scale bars: 10 µm; zoom 5 µm.

D: Co-localisation between *bcd* and Me31B::GFP particles in the apical cytoplasm early and mid n.c. 14. N = 5 embryos.

E: P body number in the apical cytoplasm between early n.c. 14 and mid n.c. 14. N = 5 embryos.

F: Number of bcd particles present in the apical cytoplasm through early n.c. 14, mid n.c. 14, and late n.c. 14. N = 5 embryos.

D-F: * $p < 0.05$; *** $p < 10^{-3}$.

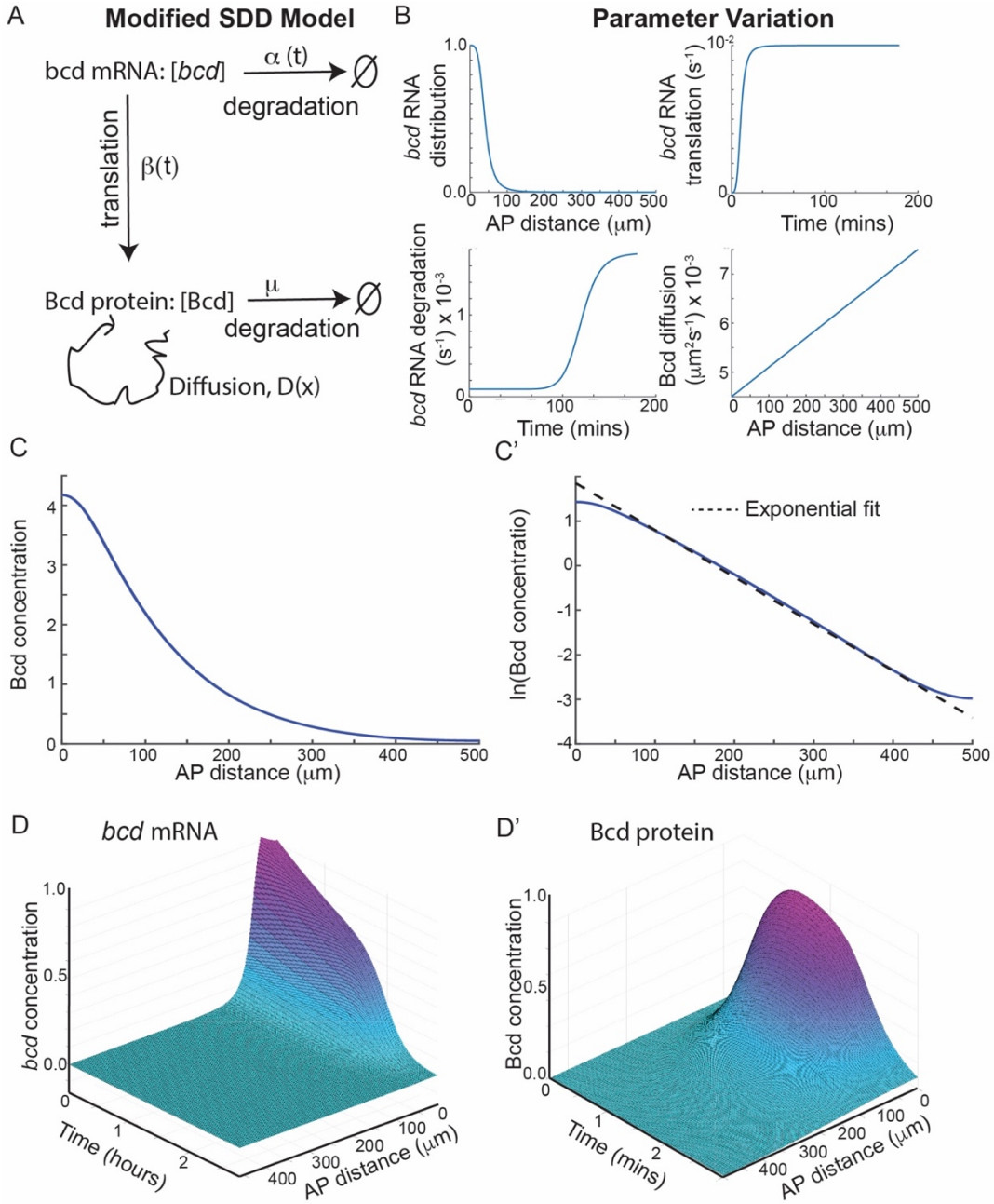

Figure 7: Modified SDD model of Bcd gradient formation

A: Model schematic, outlining parameters defining bcd and Bcd production, degradation and movement.

B: Initial conditions (i) and parameter variation (ii-iv) over time or space within the model.

C: Bcd concentration after 120 minutes in the simulation. C': Same as C on log-plot, with an exponential fit shown with the dashed black line. Dashed line has decay length of 85 μm.

D: Normalised concentration in space and time for *bcd* (D) and Bcd protein (D').

References

1. Turing AM. The chemical basis of morphogenesis. Bulletin of mathematical biology. 1952;52:153-97.
2. Ashe HL, Briscoe J. The interpretation of morphogen gradients. Development. 2006;133:385-94.
3. Driever W, Nüsslein-Volhard C. A gradient of bicoid protein in Drosophila embryos. Cell. 1988;54:83-93.
4. Gregor T, Tank DW, Wieschaus EF, Bialek W. Probing the limits to positional information. Cell. 2007;130:153-64.
5. Rivera-Pomar R, Lu X, Perrimon N, Taubert H, Jäckle H. Activation of posterior gap gene expression in the Drosophila blastoderm. Nature. 1995;376:253-6.
6. Struhl G, Struhl K, Macdonald PM. The gradient morphogen bicoid is a concentration-dependent transcriptional activator. Cell. 1989;57:1259-73.
7. Gregor T, Wieschaus EF, McGregor AP, Bialek W, Tank DW. Stability and nuclear dynamics of the bicoid morphogen gradient. Cell. 2007;130:141-52.
8. Houchmandzadeh B, Wieschaus E, Leibler S. Establishment of developmental precision and proportions in the early Drosophila embryo. Nature. 2002;415:798-802.
9. Wartlick O, Kicheva A, Gonzalez-Gaitan M. Morphogen gradient formation. Cold Spring Harb Perspect Biol. 2009;1:a001255.
10. Durrieu L, Kirrmaier D, Schneidt T, Kats I, Raghavan S, Hufnagel L, et al. Bicoid gradient formation mechanism and dynamics revealed by protein lifetime analysis. Mol Syst Biol. 2018;14:e8355.
11. Huang A, Saunders TE. A matter of time: Formation and interpretation of the Bicoid morphogen gradient. Curr Top Dev Biol. 2020;137:79-117.
12. Spirov A, Fahmy K, Schneider M, Frei E, Noll M, Baumgartner S. Formation of the bicoid morphogen gradient: an mRNA gradient dictates the protein gradient. Development. 2009;136:605-14.
13. Ali-Murthy Z, Kornberg TB. Bicoid gradient formation and function in the Drosophila pre-syncytial blastoderm. Elife. 2016;5:e13222.
14. Coppey M, Berezhkovskii AM, Kim Y, Boettiger AN, Shvartsman SY. Modeling the bicoid gradient: diffusion and reversible nuclear trapping of a stable protein. Dev Biol. 2007;312:623-30.
15. Grimm O, Coppey M, Wieschaus E. Modelling the Bicoid gradient. Development. 2010;137:2253-64.
16. Lucas T, Ferraro T, Roelens B, De Las Heras Chanes J, Walczak AM, Coppey M, et al. Live imaging of bicoid-dependent transcription in Drosophila embryos. Curr Biol. 2013;23:2135-9.
17. Bergmann S, Sandler O, Sberro H, Shnider S, Schejter E, Shilo BZ, et al. Pre-steady-state decoding of the Bicoid morphogen gradient. PLoS Biol. 2007;5:e46.
18. Johnston DS, Driever W, Berleth T, Richstein S, Nüsslein-Volhard C. Multiple steps in the localization of bicoid RNA to the anterior pole of the Drosophila oocyte. Development. 1989;107(Supplement):13-9.
19. St Johnston D, Nüsslein-Volhard C. The origin of pattern and polarity in the Drosophila embryo. Cell. 1992;68:201-19.
20. Weil TT, Forrest KM, Gavis ER. Localization of bicoid mRNA in late oocytes is maintained by continual active transport. Dev Cell. 2006;11:251-62.

21. Weil TT, Parton R, Davis I, Gavis ER. Changes in bicoid mRNA Anchoring Highlight Conserved Mechanisms during the Oocyte-to-Embryo Transition. Current Biology. 2008;18:1055-61.
22. Kronja I, Yuan B, Eichhorn SW, Dzeyk K, Krijgsveld J, Bartel DP, et al. Widespread changes in the posttranscriptional landscape at the Drosophila oocyte-to-embryo transition. Cell Rep. 2014;7:1495-508.
23. Kronja I, Whitfield ZJ, Yuan B, Dzeyk K, Kirkpatrick J, Krijgsveld J, et al. Quantitative proteomics reveals the dynamics of protein changes during Drosophila oocyte maturation and the oocyte-to-embryo transition. Proc Natl Acad Sci U S A. 2014;111:16023-8.
24. Eichhorn SW, Subtelny AO, Kronja I, Kwasnieski JC, Orr-Weaver TL, Bartel DP. mRNA poly(A)-tail changes specified by deadenylation broadly reshape translation in Drosophila oocytes and early embryos. Elife. 2016;5:e16955.
25. Mahowald AP, Goralski TJ, Caulton JH. In vitro activation of Drosophila eggs. Developmental biology. 1983;98(2):437-45.
26. York-Andersen AH, Parton RM, Bi CJ, Bromley CL, Davis I, Weil TT. A single and rapid calcium wave at egg activation in Drosophila. Biol Open. 2015;4(4):553-60.
27. Horner VL, Wolfner MF. Mechanical stimulation by osmotic and hydrostatic pressure activates Drosophila oocytes in vitro in a calcium-dependent manner. Dev Biol. 2008;316(1):100-9.
28. Hu Q, Wolfner MF. The Drosophila Trpm channel mediates calcium influx during egg activation. Proc Natl Acad Sci U S A. 2019;116(38):18994-9000.
29. Aviles-Pagan EE, Orr-Weaver TL. Activating embryonic development in Drosophila. Semin Cell Dev Biol. 2018;84:100-10.
30. Weil TT, Parton RM, Herpers B, Soetaert J, Veenendaal T, Xanthakis D, et al. Drosophila patterning is established by differential association of mRNAs with P bodies. Nat Cell Biol. 2012;14:1305-13.
31. Sankaranarayanan M, Emenecker RJ, Wilby EL, Jahnel M, Trussina I, Wayland M, et al. Adaptable P body physical states differentially regulate bicoid mRNA storage during early Drosophila development. Dev Cell. 2021;56:2886-901 e6.
32. Hubstenberger A, Courel M, Benard M, Souquere S, Ernoult-Lange M, Chouaib R, et al. P-Body Purification Reveals the Condensation of Repressed mRNA Regulons. Mol Cell. 2017;68:144-57 e5.
33. Standart N, Weil D. P-bodies: cytosolic droplets for coordinated mRNA storage. Trends in Genetics. 2018;34:612-26.
34. Riggs CL, Kedersha N, Ivanov P, Anderson P. Mammalian stress granules and P bodies at a glance. J Cell Sci. 2020;133.
35. Xing W, Muhlrad D, Parker R, Rosen MK. A quantitative inventory of yeast P body proteins reveals principles of composition and specificity. Elife. 2020;9:e56525.
36. Luo Y, Na Z, Slavoff SA. P-Bodies: Composition, Properties, and Functions. Biochemistry. 2018;57:2424-31.
37. Bose M, Lampe M, Mahamid J, Ephrussi A. Liquid-to-solid phase transition of oskar ribonucleoprotein granules is essential for their function in Drosophila embryonic development. Cell. 2022;185:1308-24 e23.
38. Buddika K, Huang YT, Ariyapala IS, Butrum-Griffith A, Norrell SA, O'Connor AM, et al. Coordinated repression of pro-differentiation genes via P-bodies and transcription maintains Drosophila intestinal stem cell identity. Curr Biol. 2022;32:386-97 e6.

39. Pushpalatha KV, Solyga M, Nakamura A, Besse F. RNP components condense into repressive RNP granules in the aging brain. Nat Commun. 2022;13:2782.
40. Chen R, Stainier W, Dufourt J, Lagha M, Lehmann R. Direct observation of translational activation by a ribonucleoprotein granule. Nature Cell Biology. 2024;26:1322-35.
41. Ramat A, Haidar A, Garret C, Simonelig M. Spatial organization of translation and translational repression in two phases of germ granules. Nature Communications. 2024;15:8020.
42. Parker R, Sheth U. P bodies and the control of mRNA translation and degradation. Mol Cell. 2007;25:635-46.
43. Davidson A, Parton RM, Rabouille C, Weil TT, Davis I. Localized Translation of gurken/TGF-alpha mRNA during Axis Specification Is Controlled by Access to Orb/CPEB on Processing Bodies. Cell Rep. 2016;14:2451-62.
44. Wang M, Ly M, Lugowski A, Laver JD, Lipshitz HD, Smibert CA, et al. ME31B globally represses maternal mRNAs by two distinct mechanisms during the Drosophila maternal-to-zygotic transition. Elife. 2017;6:e27891.
45. St Johnston D. Polarity and axis formation in the Drosophila female germ line. Curr Top Dev Biol. 2023;154:73-97.
46. Trovisco V, Belaya K, Nashchekin D, Irion U, Sirinakis G, Butler R, et al. bicoid mRNA localises to the Drosophila oocyte anterior by random Dynein-mediated transport and anchoring. Elife. 2016;5:e17537.
47. Weil TT, Xanthakis D, Parton R, Dobbie I, Rabouille C, Gavis ER, et al. Distinguishing direct from indirect roles for bicoid mRNA localization factors. Development. 2010;137:169-76.
48. Porcher A, Abu-Arish A, Huart S, Roelens B, Fradin C, Dostatni N. The time to measure positional information: maternal hunchback is required for the synchrony of the Bicoid transcriptional response at the onset of zygotic transcription. Development. 2010;137:2795-804.
49. Athilingam T, Nelanuthala AVS, Breen C, Karedla N, Fritzsche M, Wohland T, et al. Long-range formation of the Bicoid gradient requires multiple dynamic modes that spatially vary across the embryo. Development. 2024;151:dev202128.
50. Tanenbaum ME, Gilbert LA, Qi LS, Weissman JS, Vale RD. A protein-tagging system for signal amplification in gene expression and fluorescence imaging. Cell. 2014;159:635-46.
51. Pichon X, Bastide A, Safieddine A, Chouaib R, Samacoits A, Basyuk E, et al. Visualization of single endogenous polysomes reveals the dynamics of translation in live human cells. J Cell Biol. 2016;214:769-81.
52. Wang C, Han B, Zhou R, Zhuang X. Real-Time Imaging of Translation on Single mRNA Transcripts in Live Cells. Cell. 2016;165:990-1001.
53. Wu B, Eliscovich C, Yoon YJ, Singer RH. Translation dynamics of single mRNAs in live cells and neurons. Science. 2016;352:1430-5.
54. Yan X, Hoek TA, Vale RD, Tanenbaum ME. Dynamics of Translation of Single mRNA Molecules In Vivo. Cell. 2016;165:976-89.
55. Dufourt J, Bellec M, Trullo A, Dejean M, De Rossi S, Favard C, et al. Imaging translation dynamics in live embryos reveals spatial heterogeneities. Science. 2021;372:840-4.

854 56. Vinter DJ, Hoppe C, Minchington TG, Sutcliffe C, Ashe HL. Dynamics of
855 hunchback translation in real-time and at single-mRNA resolution in the Drosophila
856 embryo. Development. 2021;148:dev196121.
857 57. Blake LA, De La Cruz A, Wu B. Imaging spatiotemporal translation regulation in
858 vivo. Seminars in Cell & Developmental Biology. 2024;154:155-64.
859 58. Little SC, Tkacik G, Kneeland TB, Wieschaus EF, Gregor T. The formation of the
860 Bicoid morphogen gradient requires protein movement from anteriorly localized mRNA.
861 PLoS Biol. 2011;9:e1000596.
862 59. Gregor T, Wieschaus EF, McGregor AP, Bialek W, Tank DW. Stability and nuclear
863 dynamics of the bicoid morphogen gradient. Cell. 2007;130(1):141-52.
864 60. Bellec M, Chen R, Dhayni J, Trullo A, Avinens D, Karaki H, et al. Boosting the
865 toolbox for live imaging of translation. RNA. 2024;30(10):1374-94.
866 61. Tadros W, Lipshitz HD. The maternal-to-zygotic transition: a play in two acts.
867 Development. 2009;136(18):3033-42.
868 62. Lasko P. mRNA localization and translational control in Drosophila oogenesis.
869 Cold Spring Harb Perspect Biol. 2012;4(10).
870 63. Riggs CL, Kedersha N, Ivanov P, Anderson P. Mammalian stress granules and P
871 bodies at a glance. J Cell Sci. 2020;133(16).
872 64. Xing W, Muhlrad D, Parker R, Rosen MK. A quantitative inventory of yeast P body
873 proteins reveals principles of composition and specificity. Elife. 2020;9.
874 65. Hubstenberger A, Courel M, Benard M, Souquere S, Ernoult-Lange M, Chouaib R,
875 et al. P-Body Purification Reveals the Condensation of Repressed mRNA Regulons. Mol
876 Cell. 2017;68(1):144-57 e5.
877 66. Weil TT, Parton RM, Herpers B, Soetaert J, Veenendaal T, Xanthakis D, et al.
878 Drosophila patterning is established by differential association of mRNAs with P bodies.
879 Nat Cell Biol. 2012;14(12):1305-13.
880 67. Kronja I, Whitfield ZJ, Yuan B, Dzeyk K, Kirkpatrick J, Krijgsveld J, et al.
881 Quantitative proteomics reveals the dynamics of protein changes during Drosophila
882 oocyte maturation and the oocyte-to-embryo transition. Proc Natl Acad Sci U S A.
883 2014;111(45):16023-8.
884 68. Driever W, Nüsslein-Volhard C. A gradient of bicoid protein in Drosophila
885 embryos. Cell. 1988;54(1):83-93.
886 69. Bose M, Rankovic B, Mahamid J, Ephrussi A. An architectural role of specific
887 RNA-RNA interactions in oskar granules. Nat Cell Biol. 2024;26:1934-42.
888 70. Alberti S, Gladfelter A, Mittag T. Considerations and Challenges in Studying
889 Liquid-Liquid Phase Separation and Biomolecular Condensates. Cell. 2019;176:419-34.
890 71. McSwiggen DT, Mir M, Darzacq X, Tjian R. Evaluating phase separation in live
891 cells: diagnosis, caveats, and functional consequences. Genes Dev. 2019;33:1619-34.
892 72. Gao Y, Li X, Li P, Lin Y. A brief guideline for studies of phase-separated
893 biomolecular condensates. Nature Chemical Biology. 2022;18:1307-18.
894 73. Mahowald AP, Goralski TJ, Caulton JH. In vitro activation of Drosophila eggs.
895 Developmental biology. 1983;98:437-45.
896 74. Horner VL, Wolfner MF. Mechanical stimulation by osmotic and hydrostatic
897 pressure activates Drosophila oocytes in vitro in a calcium-dependent manner. Dev
898 Biol. 2008;316:100-9.

75. Von Stetina JR, Tranguch S, Dey SK, Lee LA, Cha B, Drummond-Barbosa D. alpha-Endosulfine is a conserved protein required for oocyte meiotic maturation in Drosophila. Development. 2008;135:3697-706.
76. Rangone H, Bond L, Weil TT, Glover DM. Greatwall-Endos-PP2A/B55(Twins) network regulates translation and stability of maternal transcripts in the Drosophila oocyte-to-embryo transition. Open Biol. 2024;14:240065.
77. Little SC, Tkacik G, Kneeland TB, Wieschaus EF, Gregor T. The formation of the Bicoid morphogen gradient requires protein movement from anteriorly localized mRNA. PLoS Biol. 2011;9(3):e1000596.
78. Surdej P, Jacobs-Lorena M. Developmental regulation of bicoid mRNA stability is mediated by the first 43 nucleotides of the 3′ untranslated region. Molecular and cellular biology. 1998;18:2892-900.
79. Wang C-Y, Wang Y-T, Hsiao W-Y, Wang S-W. Involvement of fission yeast Pdc2 in RNA degradation and P-body function. Rna. 2017;23:493-503.
80. Eichler CE, Hakes AC, Hull B, Gavis ER. Compartmentalized oskar degradation in the germ plasm safeguards germline development. Elife. 2020;9:e49988.
81. Forbes Beadle L, Love JC, Shapovalova Y, Artemev A, Rattray M, Ashe HL. Combined modelling of mRNA decay dynamics and single-molecule imaging in the Drosophila embryo uncovers a role for P-bodies in 5' to 3' degradation. PLoS Biol. 2023;21:e3001956.
82. He F, Saunders TE, Wen Y, Cheung D, Jiao R, ten Wolde PR, et al. Shaping a morphogen gradient for positional precision. Biophys J. 2010;99:697-707.
83. Baumgartner S. Seeing is believing: the Bicoid protein reveals its path. Hereditas. 2018;155:28.
84. Shlemov A, Alexandrov T, Golyandina N, Holloway D, Baumgartner S, Spirov AV. Quantification reveals early dynamics in Drosophila maternal gradients. PLoS One. 2021;16:e0244701.
85. Kramer S. Simultaneous detection of mRNA transcription and decay intermediates by dual colour single mRNA FISH on subcellular resolution. Nucleic Acids Res. 2017;45:e49.
86. Patel PH, Barbee SA, Blankenship JT. GW-Bodies and P-Bodies Constitute Two Separate Pools of Sequestered Non-Translating RNAs. PLoS One. 2016;11:e0150291.
87. Hakes AC, Gavis ER. Plasticity of Drosophila germ granules during germ cell development. PLoS Biol. 2023;21(4):e3002069.
88. Weil TT, Parton RM, Davis I. Preparing individual Drosophila egg chambers for live imaging. J Vis Exp. 2012;60:3679.
89. Abbaszadeh EK, Gavis ER. Fixed and live visualization of RNAs in Drosophila oocytes and embryos. Methods. 2016;98:34-41.
90. Bellec M, Chen R, Dhayni J, Trullo A, Avinens D, Karaki H, et al. Boosting the toolbox for live imaging of translation. RNA. 2024;30:1374-94.
91. Bolte S, Cordelieres FP. A guided tour into subcellular colocalization analysis in light microscopy. J Microsc. 2006;224:213-32.
92. Hu Q, Wolfner MF. The Drosophila Trpm channel mediates calcium influx during egg activation. Proc Natl Acad Sci U S A. 2019;116:18994-9000.